ARTICLE

A Recurrent Gain-of-Function Mutation in *CLCN6*, Encoding the ClC-6 Cl^-/H^+-Exchanger, Causes Early-Onset Neurodegeneration

Maya M. Polovitskaya,[1,2,10] Carlo Barbini,[1,2,10] Diego Martinelli,[3,10] Frederike L. Harms,[4] F. Sessions Cole,[5] Paolo Calligari,[6] Gianfranco Bocchinfuso,[6] Lorenzo Stella,[6] Andrea Ciolfi,[3] Marcello Niceta,[3] Teresa Rizza,[3] Marwan Shinawi,[7] Kathleen Sisco,[7] Jessika Johannsen,[8] Jonas Denecke,[8] Rosalba Carrozzo,[3] Daniel J. Wegner,[5] Kerstin Kutsche,[4] Marco Tartaglia,[3,11,*] and Thomas J. Jentsch[1,2,9,11,*]

Summary

Dysfunction of the endolysosomal system is often associated with neurodegenerative disease because postmitotic neurons are particularly reliant on the elimination of intracellular aggregates. Adequate function of endosomes and lysosomes requires finely tuned luminal ion homeostasis and transmembrane ion fluxes. Endolysosomal CLC Cl^-/H^+ exchangers function as electric shunts for proton pumping and in luminal Cl^- accumulation. We now report three unrelated children with severe neurodegenerative disease, who carry the same *de novo* c.1658A>G (p.Tyr553Cys) mutation in *CLCN6*, encoding the late endosomal Cl^-/H^+-exchanger ClC-6. Whereas *Clcn6*$^{-/-}$ mice have only mild neuronal lysosomal storage abnormalities, the affected individuals displayed severe developmental delay with pronounced generalized hypotonia, respiratory insufficiency, and variable neurodegeneration and diffusion restriction in cerebral peduncles, midbrain, and/or brainstem in MRI scans. The p.Tyr553Cys amino acid substitution strongly slowed ClC-6 gating and increased current amplitudes, particularly at the acidic pH of late endosomes. Transfection of ClC-6^{Tyr553Cys}, but not ClC-6^{WT}, generated giant LAMP1-positive vacuoles that were poorly acidified. Their generation strictly required ClC-6 ion transport, as shown by transport-deficient double mutants, and depended on Cl^-/H^+ exchange, as revealed by combination with the uncoupling p.Glu200Ala substitution. Transfection of either ClC-6$^{Tyr553Cys/Glu200Ala}$ or ClC-6^{Glu200Ala} generated slightly enlarged vesicles, suggesting that p.Glu200Ala, previously associated with infantile spasms and microcephaly, is also pathogenic. Bafilomycin treatment abrogated vacuole generation, indicating that H^+-driven Cl^- accumulation osmotically drives vesicle enlargement. Our work establishes mutations in *CLCN6* associated with neurological diseases, whose spectrum of clinical features depends on the differential impact of the allele on ClC-6 function.

Introduction

The function of endosomes and lysosomes depends critically on the transport of ions across their limiting membranes. For example, the luminal concentration of ions, prominently including H^+, influences luminal receptor-ligand interactions, lysosomal enzyme activities, and membrane budding and fusion.[1–3] Release of calcium from vesicles is important for their fusion with other vesicles or the plasma membrane,[2,4] and transmembrane transport of small organic molecules is often coupled to ion gradients, as illustrated by the uptake of neurotransmitters into synaptic vesicles.[5] The functional relevance of vesicular ion transport and the requirement of its fine tuning are documented by the large number of channels and transporters known to be expressed in lysosomal and endosomal membranes.[2,6–8] Consistent with its relevant role in cell physiology, disruption or functional alteration of vesicular ion transport is associated with a number of human diseases.[2,7–9] In particular, loss-of-function mutations in each of the genes that encode the nine members of the voltage-dependent chloride channel and transporter (CLC) family has been documented to cause pathology in humans and/or mice.[7,9] Given that most *CLCN* genes show a wide tissue distribution, mutations changing their function often cause multi-system disorders.[9]

CLC proteins (encoded by *CLCN* genes) assemble to dimers that function either as Cl^- channels or anion/proton exchangers with one permeation pathway per monomer.[9–12] ClC-3 to ClC-7 are Cl^-/H^+-exchangers in the endolysosomal pathway of mammalian cells where they modulate the luminal ion composition and probably the electrical potential of the respective vesicular compartment.[9] They share key biophysical properties, such as

[1]Leibniz-Forschungsinstitut für Molekulare Pharmakologie (FMP), 13125 Berlin, Germany; [2]Max-Delbrück-Centrum für Molekulare Medizin (MDC), 13125 Berlin, Germany; [3]Genetics and Rare Diseases Research Division, Ospedale Pediatrico Bambino Gesù, IRCCS, 00146 Rome, Italy; [4]Institute for Human Genetics, University Medical Center Hamburg-Eppendorf, 20246 Hamburg, Germany; [5]Division of Newborn Medicine, Edward Mallinckrodt Department of Pediatrics, Washington University School of Medicine, and St. Louis Children's Hospital, St. Louis, MO 63110, USA; [6]Department of Chemical Science and Technologies, University "Tor Vergata," 00133 Rome, Italy; [7]Division of Genetics and Genomic Medicine, Edward Mallinckrodt Department of Pediatrics, Washington University School of Medicine, and St. Louis Children's Hospital, St. Louis, MO 63110, USA; [8]Children's Hospital, University Medical Center Hamburg-Eppendorf, 20246 Hamburg, Germany; [9]NeuroCure Cluster of Excellence, Charité Universitätsmedizin, 10117 Berlin, Germany
[10]These authors contributed equally
[11]These authors contributed equally
*Correspondence: marco.tartaglia@opbg.net (M.T.), jentsch@fmp-berlin.de (T.J.J.)
https://doi.org/10.1016/j.ajhg.2020.11.004.

electrogenic $2Cl^-/H^+$-exchange, activation by cytoplasmic positive voltages, and inhibition by acidic luminal pH, and show partially overlapping cellular and subcellular expression patterns. In humans, loss-of-function of several vesicular CLCs leads to diverse phenotypes. These range from impaired renal endocytosis and kidney stones (ClC-5)[13,14] (MIM: 300009), to intellectual disability (ID) and epilepsy (ClC-4)[15,16] (MIM: 302910), to severe lysosomal storage disease and osteopetrosis (ClC-7, or its obligatory β-subunit OSTM1)[17–19] (MIM: 611490, 259720). However, the mechanisms by which loss- or gain-of-function mutations in the respective genes cause disease remain poorly understood.

CLCN6 (MIM: 602726) encodes a Cl^-/H^+-exchanger that is predominantly found in late endosomes of the nervous system.[20–22] Whereas *Clcn6* disruption in mice leads to mild lysosomal storage mainly in axon initial segments,[21] no convincing link of *CLCN6* mutations to human disease has been established to date. We here report the same *de novo CLCN6* missense variant, c.1658A>G (p.Tyr553Cys), in three unrelated children sharing a consistent clinical phenotype characterized by developmental delay (DD) with early-onset regression, severe generalized hypotonia, respiratory insufficiency, and early-onset cerebral atrophy and neurogenic bladder in two of the probands. The severe phenotype in these individuals contrasts with the mild phenotype in $Clcn6^{-/-}$ mice and normal heterozygous $Clcn6^{+/-}$ mice,[21,23] suggesting a specific consequence of the amino acid substitution on ClC-6 function. Electrophysiological analysis of heterologously expressed, partially cell surface-targeted ClC-6 revealed that the pathogenic Tyr-to-Cys substitution substantially increases current amplitudes, which, unlike those of the wild-type (WT) exchanger, are not reduced at the acidic pH prevalent in late endosomes. Transfection of the ClC-6 mutant, but not WT, into various cell lines resulted in the appearance of dramatically enlarged lysosome-related vesicles. Their generation depended on Cl^-/H^+ exchange of the ClC-6 mutant and on the activity of the H^+-ATPase, suggesting an important role of luminal Cl^- accumulation and subsequent osmotic swelling. Together with previous reports on a "likely pathogenic" ClC-6 p.Glu200Ala variant associated with infantile spasms,[24,25] our work now firmly establishes that different mutations in *CLCN6* can underlie various neurological diseases.

Subjects and Methods

Subjects

This project was approved by the local Institutional Ethical Committee of the Ospedale Pediatrico Bambino Gesù (1702_OPBG_2018), Rome, and the Ethics Committee of the Hamburg Medical Chamber (PV3802). Subjects 1 and 2 were analyzed in the frame of a research project dedicated to undiagnosed patients, while subject 3 was referred for diagnostic genetic testing. Clinical data and biological material were collected, stored, and used according to procedures in accordance with the ethical standards of the declaration of Helsinki protocols, with signed informed consents from the participating families. Explicit permission was obtained to publish the photographs of the subjects as shown in Figure 1.

Whole-Exome Sequencing, Variant Filtering, and Variant Validation

Whole-exome sequencing (WES) was performed using genomic DNA obtained from leukocytes. A trio-based strategy was used in all cases. Target enrichment kits, sequencing platforms, WES statistics, and data output are summarized in Table S1. WES data processing, sequence alignment to GRCh37, variant filtering and prioritization by allele frequency, predicted functional impact, and inheritance models were performed as previously described[26,27] and reported as Supplemental Subjects and Methods. The *de novo* origin of the *CLCN6* mutation was confirmed by Sanger sequencing in all cases (primer sequences available on request).

Cell Culture

HeLa cells and human primary fibroblasts of affected subjects and healthy age-matched control subjects, obtained from skin biopsies, were grown in Dulbecco's modified Eagle medium supplemented with 10% FCS and 1% Pen/Strep. U2OS LAMP1-GFP cells[28] were cultured in McCoy medium supplemented with 10% FCS and 1% Pen/Strep.

Electrophysiological Analysis of Transfected Cells

The expression constructs had coding sequence for GFP fused to the 5′ end of human ClC-6 cDNA as described.[22] CHO-K1 cells were used for expression because they almost lack endogenous depolarization-induced anion currents,[22] presumably because they lack ClC-5 expression.[29] CHO-K1 cells were maintained in Ham's F12 Medium (PAN Biotech) supplemented with 10% FBS (PAN Biotech) and 1% Pen/Strep at 37°C and 5% CO_2. For patch clamp recording, cells were transfected using FuGENE (Promega) in 6-well plate format with 3 mg DNA per well at 3:1 reagent:DNA ratio. Currents were measured 48–72 h after transfection. Trypsin-treated cells were seeded onto uncoated glass coverslips 1–6 h before recording.

Whole-cell patch clamp measurements of transfected cells (identified by GFP fluorescence) were performed at room temperature using MultiClamp 700B patch-clamp amplifier/Digidata 1550B digitizer and pClamp 10 software (Molecular Devices). Patch pipettes were filled with solution containing (in mM) 140 CsCl, 5 EGTA, 1 $MgCl_2$, 10 HEPES, pH adjusted to 7.2 with CsOH (275 mOsm), and had resistance of 3–6 MΩ. Bath solution contained (in mM) 150 NaCl, 6 KCl, 1 $MgCl_2$, 1.5 $CaCl_2$, 10 glucose, 10 HEPES, pH adjusted to 7.5 with NaOH (320 mOsm). In some experiments, NaCl was substituted with an equimolar amount of NaI. Bath solutions with pH 5.5, 6.5, and 8.5 were buffered with 10 mM MES or Tris, as appropriate. The voltage clamp protocol consisted of a 2 s steps from −100 to +120 mV in 20-mV increments from a holding potential of −30 mV applied every 5 s. Recordings were low pass-filtered at 6 kHz and sampled at 10 kHz.

Immunofluorescence of Transfected Cells

HeLa cells were transfected 2 days prior to immunostaining using FuGENE, according to manufacturer's instructions. For co-staining of ClC-6 with LAMP1 or cathepsin D, cells were fixed

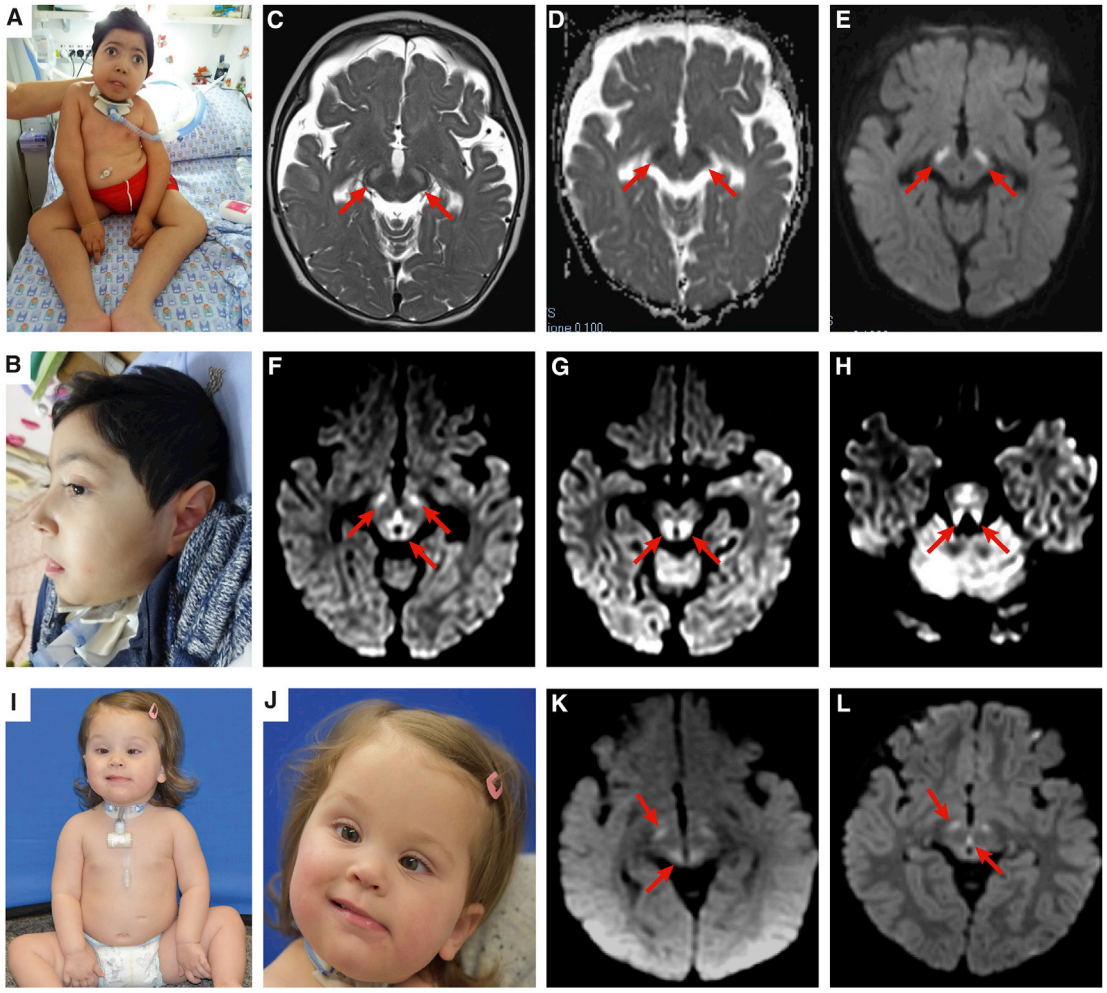

Figure 1. Clinical and MRI Features of the Subjects Heterozygous for the *De Novo CLCN6* c.1658A>G Missense Change
(A and B) Clinical features of subject 1, showing mild dysmorphic features, severe generalized hypotonia, blindness, and tracheostomy to treat respiratory insufficiency.
(C–E) MRI scan of subject 1 at 10 months: (C) axial T2 weighted images; (D) ADC and (E) DWI images: moderate fronto-temporal atrophy, bilateral symmetrical brainstem lesions (cerebral peduncles, red arrows), with diffusion restriction at ADC and DWI sequences.
(F–H) MRI scans of subject 2 at the age of 18 months (DWI images) show bilateral diffusion restriction (red arrows) in cerebral peduncles and dorsal midbrain (F), dorsal brainstem (G), and superior cerebellar peduncles (H).
(I and J) Clinical features of subject 3, showing generalized hypotonia and tracheostomy and eye esotropia.
(K and L) MRI scans of subject 3 showing bilateral diffusion restriction in the cerebral peduncles and periaqueductal region at age 7 months (K) and 22 months (L).

with 4% paraformaldehyde in phosphate-buffered saline (PBS) for 15 min. Then, cells were incubated with 25 mM glycine in PBS for 5 min and permeabilized with 0.05% saponin in PBS for 10 min. All antibodies and DAPI dye were applied in PBS/0.05% saponin/3% BSA. Untagged ClC-6 was immunostained with a knock-out controlled rabbit antibody against the ClC-6 C terminus (6C3)[22] and GFP-ClC-6 with chicken anti-GFP antibody (Aves). Other antibodies used were mouse anti-LAMP1 (H4A3, Abcam) and rabbit anti-cathepsin D (219361, EMD Millipore). Secondary antibodies had been raised in goat and conjugated to Alexa Fluor 488, 555, or 633 (Molecular Probes). Images were acquired with an LSM880 laser scanning confocal microscope with a 63 × 1.4 numerical aperture oil-immersion lens (Zeiss).

LysoTracker Staining

10^5 U2OS LAMP1-GFP cells were plated 48 h before imaging on 35 mm MatTek glass-bottom dishes. Cells were transfected after 4 h with FuGene. Before imaging, cells were incubated for 30 min in 50 nM LysoTracker Red (Thermo Fisher) in complete growth medium. Cells were then washed 2× with PBS and imaged in live imaging buffer containing (in mM) 135 NaCl, 5 KCl, 1 $CaCl_2$, 1 $MgCl_2$, 10 glucose, 25 HEPES (pH 7.4). Images were taken with a LSM880 confocal microscope system and a Plan-Apochromat 63×/1.40 oil objective. LAMP1-GFP fluorescence was excited at 488 nm and detected at 535 nm, LysoTracker Red fluorescence was excited at 555 nm and detected at 580 nm. Imaging was conducted at room temperature and for less than 30 min.

Vacuolar pH Measurements

10^5 HeLa cells were plated 48 h before imaging on 35 mm MatTek glass-bottom dishes. Cells were transfected after 4 h with FuGENE. On the following day, cells were loaded overnight with 0.5 mg/mL OregonGreen 488 Dextran (Thermo Fisher)

in growth medium at 37°C/5% CO_2. Cells were washed 2× with PBS and incubated for additional 2 h to chase the dye into lysosomes. After washing once with PBS, cells were imaged in live imaging buffer (see above). Images were taken with an inverted Axiovert II microscope coupled to a PolyV monochromator (TILL photonics, FEI) and a Sensicam CCD camera (PCO). The ratiometric fluorophore was intermittently excited at 440 nm and 488 nm and the emitted light was filtered with a 535 ± 20 nm filter (AHF). At the end of each experiment, the pH-sensitive fluorophore was calibrated to different pH values ranging from 4 to 6.5. The clamping solutions contained (in mM) 5 NaCl, 135 KCl, 1 $CaCl_2$, 1.2 $MgSO_4$, 10 glucose, 25 of either HEPES or MES depending on the pH value. The addition of 10μM monensin and 10 μM nigericin enabled the equilibration of the vesicular pH with that of the applied buffer. Cells were incubated for at least 5 min in the equilibration buffer before the measurements were started. Regions of interest were drawn manually. After background subtraction, the 488/440 fluorescence ratios in these regions were interpolated to the ones obtained by a Boltzmann equation-sigmoidal fit obtained from the calibration curve and converted to pH values. The measurements were obtained from three independent experiments performed at room temperature, each with an own calibration curve.

Endocytic Uptake of Alexa Fluor Dextran

1×10^5 U2OS LAMP1-GFP or HeLa cells were plated 48 h before imaging on 35 mm MatTek glass-bottom dishes. Cells were transfected after 4 h with FuGENE. On the following day cells were loaded overnight with 0.5 mg/mL dextran-coupled Alexa Fluor 488 (HeLa) or 546 (U2OS) (Thermo Fisher) in growth medium in a 37°C/5% CO_2 atmosphere. On the next day, cells were incubated after a PBS wash in complete medium for 2 h and then imaged in live imaging buffer. Images were taken with a LSM880 confocal microscope system and a Plan-Apochromat 63×/1.40 oil objective. LAMP1-GFP and AlexaFluor488 fluorescence was excited at 488 nm and detected at 535 nm, while AlexaFluor546 fluorescence was excited at 555 nm and detected at 580 nm.

Live Cell Imaging of Vacuole Formation and Resolution

5×10^4–1×10^5 U2OS LAMP1-GFP cells were plated on μ-slide 8 well (IBIDI) and transfected after 2 h with FuGENE. 4 h after transfection, cells were washed once with PBS, covered with live imaging buffer plus 10% FCS, and imaged with a Nikon-CSU Spinning Disk Confocal microscope at 37°C in a 5% CO_2 atmosphere. LAMP1-GFP fluorescence was excited at 488 nm and detected at 535 nm. For Video S1, settings of the NIS Elements software were adjusted for acquisition with a time-lapse of 3 min for 15 h. For Video S2, the time-lapse was reduced to 1 min (total recording 5.6 h), and for Video S3, time intervals were set to 30 s (5 h recording) and bafilomycin (10 nM final) was added 1 h after start of recording.

Serum Copper Level Determination in Mice

After deep anesthesia, blood was taken from hearts of 9- to 23-week-old WT and *Clcn6*$^{-/-}$ mice.[21] Serum copper concentrations were determined by ICP-MS (Synevo Central Labs).

Results

The Recurrent *De Novo CLCN6* Variant c.1658A>G (p.Tyr553Cys) Is Associated with Global DD, Generalized Hypotonia, and Respiratory Insufficiency

Three subjects from unrelated families were included in the study. In the frame of a research program dedicated to individuals affected by undiagnosed diseases ongoing at the Ospedale Pediatrico Bambino Gesù, Rome, trio-based whole-exome sequencing (WES) was performed to identify the genetic cause of a molecularly unexplained early-onset neurodegenerative disorder affecting a child (Figure 1A), who showed progressive cortical atrophy and bilateral brainstem lesions (Figures 1C–1E), severe DD, generalized hypotonia, sensory peripheral neuropathy, cortical blindness, and chronic respiratory insufficiency requiring continuous invasive ventilation (Table 1, Supplemental Note: Clinical Reports). WES statistics and data output are summarized in Table S1. WES data analysis did not find any functionally relevant variant(s) compatible with known Mendelian disorders based on the expected inheritance model and clinical presentation, and a *de novo* missense change, c.1658A>G (p.Tyr553Cys), in *CLCN6* (GenBank: NM_001286.4) was identified as the only strong candidate underlying the disease. Two additional individuals (subjects 2 and 3) sharing the same *de novo* missense change in *CLCN6* and a similar clinical condition were successively identified by using the web tool GeneMatcher.[30] Clinical, laboratory, and brain imaging data of all subjects are summarized in Tables 1 and S2. All three individuals had been investigated genetically because of an unclassified and severe neurodegenerative disorder. Subject 2, who died at the age of 23 months, presented with severe hypotonia, moderate DD with psychomotor and neurodevelopmental regression, and respiratory insufficiency (Supplemental Note: Clinical Reports). Brain MRI at the age of 18 months documented mild cerebral atrophy and brainstem lesions (Figures 1F–1H). WES performed in this individual and her parents allowed identification of a *de novo* pathogenic variant in *NF1* (MIM: 613113), predicting a frameshift and introduction of a premature stop codon (c.2452delT [p.Ser818Profs*3], GenBank: NM_000267.3) (Table S1), which however could not explain the severe neurological phenotype of the subject. The third individual (Figures 1I and 1J) was an 18-month-old girl with generalized hypotonia, DD with regression, brain MRI anomalies (Figures 1K and 1L), and respiratory insufficiency requiring tracheostomy (Table 1 and Supplemental Note: Clinical Reports). WES analysis did not identify private/rare functionally relevant variants in genes associated with neurodegenerative disorders (Table S1). In all subjects, Sanger sequencing validated the *de novo* origin of the *CLCN6* missense change. Analysis of genomic DNA from primary fibroblasts obtained from a skin biopsy in subjects 1 and 3 confirmed the occurrence of the mutation, providing evidence of germline origin. The identified missense change affected a residue highly

Table 1. Summary of the Clinical Features of the Three Subjects Heterozygous for the *De Novo* c.1658A>G (p.Tyr553Cys) Substitution in *CLCN6*

Subject #	HPO Terms	1 (Family 1)	2 (Family 2)	3 (Family 3)
Ethnic background	–	European descent	European descent	European descent
Sex	–	male	female	female
Gene, variant (NM_001286.3)	–	c.1658A>G (p.Tyr553Cys) (*de novo*)	c.1658A>G (p.Tyr553Cys) (*de novo*)	c.1658A>G (p.Tyr553Cys) (*de novo*)
Age	–	alive, 6 y 4 m	deceased, 23 m	alive, 18 m
Weight (centile, z-score)	–	20.0 kg (50, −0.63)	12.6 kg (70, 0.52)	9.5 kg (20, −0.84)
Height (centile, z-score)	–	100 cm (<1, −3.62)	87 cm (64, 0.37)	74.4 cm (<1, −2.57)
BMI (centile, z-score)	–	20 (96.9, 1.9)	16.6 (67, 0.43)	17.14 (85, 1.04)
OFC (centile, z-score)	–	50 (7, −1.42)	48 cm (47, −0.07)	46.8 cm (59, +0.24)
Neurological Features				
Global developmental delay	HP:0001263	severe DD with regression	global DD with regression	global DD with regression
Motor development	HP:0001270	absence of spontaneous movements	rolling over, but no crawling, sitting and standing at 13 months	sitting unsupported at 14 months; cruises with help
Speech impairment	HP:0002167	absent language	single words	babbles, verbalizes 7 to 8 words
Muscular hypotonia	HP:0001252	generalized hypotonia; apostural quadriplegia	severe truncal hypotonia, no spasticity	generalized hypotonia (truncal > appendicular)
Movement disorder	HP:0100022	N	Y	N
Seizures	HP:0001250	N	N	N
EEG abnormality	HP:0002353	Y	Y	N
MRI scan anomalies	–	Y	Y	Y
Neurogenic bladder	HP:0000011	Y	Y	N
Abnormality of temperature regulation	HP:0004370	Y (hyperthermia)	Y (hyperthermia)	N
Other Clinical Findings				
Cardiovascular system abnormality	HP:0030680	N	N	N
Hearing abnormality	HP:0000364	N	N	N
Abnormality of vision	HP:0000504	cortical blindness	nystagmus, optic disc elevation, and neuroretinal rim pallor	optic disc elevation, alternating esotropia, and strabismic amblyopia
Abnormality of the respiratory system	HP:0002086	chronic respiratory insufficiency, tracheostomy	chronic respiratory insufficiency, tracheostomy	chronic respiratory insufficiency, tracheostomy, & ventilator dependency
Abnormality of the skin and annexa	HP:0000951	hyperhidrosis, trichorrhexis nodosa: reduced hair copper content	hyperhidrosis	N
Feeding difficulties	HP:0011968	PEG	PEG	PEG
Craniofacial features	HP:0001999	hypertelorism, arched eyebrows, long philtrum, thin upper lip	N	N
Histological Studies				
Muscle biopsy	–	mild signs of myopathy	mild signs of myopathy	abnormal variation in muscle fiber sizes with reduced type II muscle fibers
Nerve conduction anomalies	–	sensory peripheral neuropathy	sensory peripheral neuropathy	N

Complete information is provided in Table S2. N, feature absent; NA, not assessed; PEG, percutaneous endoscopic gastrostomy; Y, feature present.

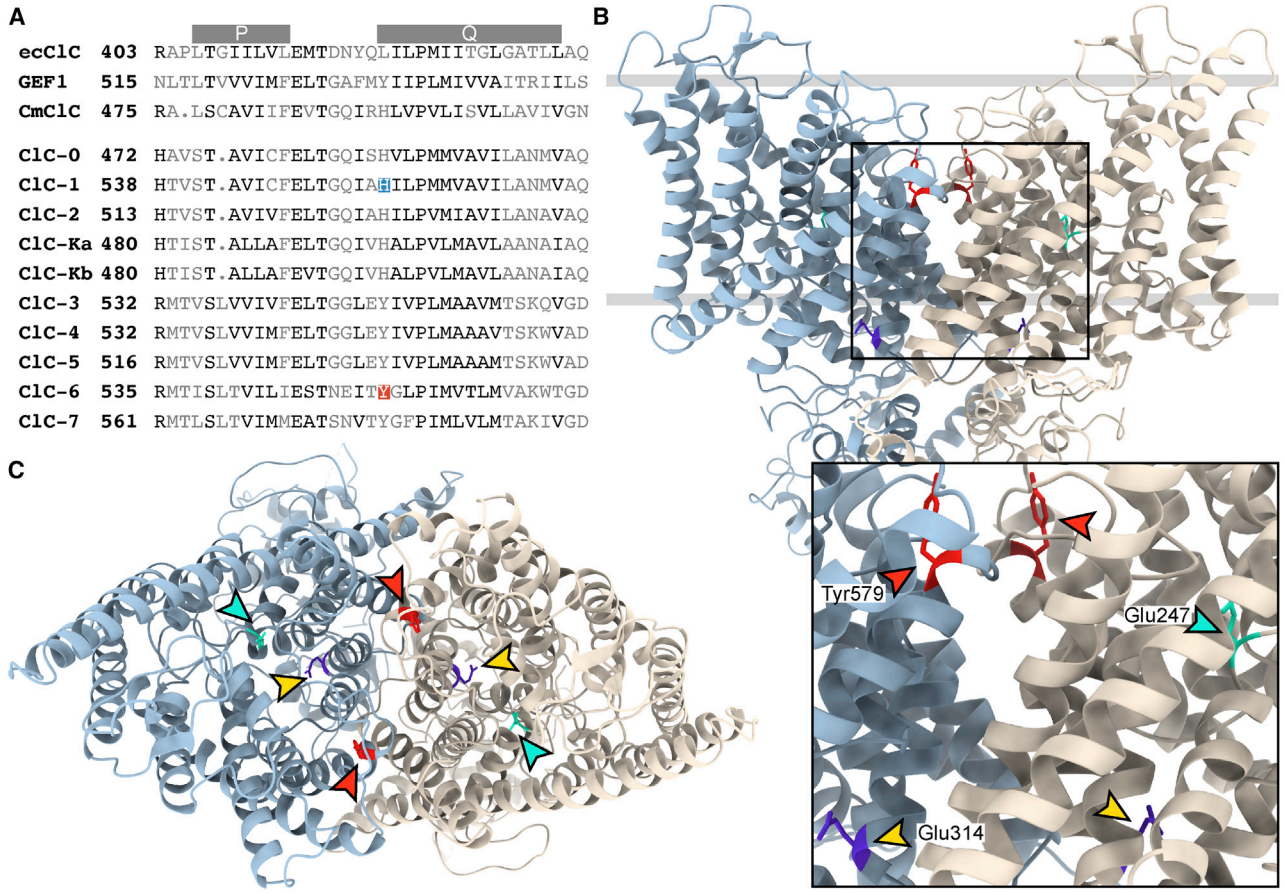

Figure 2. Conservation of Tyr^{553} among ClC-6 Orthologs and Paralogs and Its Localization in the Transporter Protein

(A) Partial alignment of the *E. coli* ecClC, yeast Gef1p, and algal cmClC Cl^-/H^+ exchangers, with the *Torpedo* channel ClC-0, the mammalian channels ClC-1, -2, -Ka, and -Kb Cl^- channels, and the mammalian ClC-3 to ClC-7 Cl^-/H^+-exchangers. ClC-6 Tyr^{553} and ClC-1 His^{555} (mutated in a subject with myotonia)[31] are highlighted. *P* and *Q* at top indicate intramembrane helices P and Q.[12]

(B) Side view of the cryo-EM structure of the human $2Cl^-/H^+$-exchanger ClC-7 (PDB: 7JM7),[32] the closest homolog of ClC-6, illustrating the position of Tyr^{579} (equivalent to ClC-6 Tyr^{553}) in the dimeric transporter. The subunits of the transporter are depicted in different colors, and the approximate position of the lipid bilayer is shown by two gray lines. ClC-7 Tyr^{579} (shown in red) is indicated by red arrowheads in the enlargement below. The gating glutamate (Glu^{247}, equivalent to ClC-6 Glu^{200}) that is located in the center of the individual ion permeation pathways of each subunit is pointed at by a cyan arrowhead. This residue is replaced by alanine in the subject described by Wang et al.[24] The proton glutamate,[33] Glu^{314}, is pointed at by a yellow arrowhead. Mutating the equivalent ClC-6 residue Glu^{267} to alanine abolishes both Cl^- and H^+ transport.[22] The large extramembrane parts correspond to the CBS-domain containing, cytosolic C termini.

(C) View of ClC-7 from above, with the relevant tyrosine residues (red) highlighted by red arrowheads. They are located at the interface of the two subunits but are not close enough to each other to allow crosslinking if mutated to cysteine. Gating and proton glutamates highlighted as in (B).

conserved among CLC proteins (Figure 2A). *In silico* predictive tools consistently classified the *CLCN6* variant as damaging/deleterious (CADD score = 28.3, SIFT score = 0.001, M-CAP score = 0.48, REVEL score = 0.96), which had not previously been reported in public (e.g., gnomAD) and in-house (see Supplemental Subjects and Methods) databases. Of note, a missense mutation (p.His555Asn) at the equivalent position in *CLCN1* had been found in a subject with myotonia,[31] further supporting the functional relevance of the recurrent *de novo* missense change.

Overall, the probands showed a common clinical phenotype characterized by DD with early-onset regression and severe generalized hypotonia and respiratory insufficiency. Besides brain atrophy, in two out of the three affected individuals, brain imaging revealed consistent and rare abnormalities in the three subjects, such as bilateral diffusion restriction in cerebral peduncles, dorsal brainstem, and/or dorsal midbrain, and additionally in superior cerebellar peduncles in subject 2 (Figure 1, Tables 1 and S2). These MRI signal abnormalities were detected at the age of 10, 18, and 7 months in subjects 1, 2, and 3, respectively (Table S2). Additional clinical features of the disorder included severe ID, mild cerebral atrophy, hyperhidrosis, myopathic changes in muscle biopsy, and overt peripheral sensory neuropathy as detected by nerve conduction assessment in subjects 1 and 2, with subject 3 showing absence of reflexes without significant changes revealed by electrophysiology studies. Neurogenic bladder was observed in

subjects 1 and 2, indicating involvement of autonomic pathways. Of note, the presence of cerebral atrophy, hypotonia, peripheral neuropathy, and bladder dysfunction, and the occurrence of bilateral subdural chronic hematomas, trichorexis nodosa, and bladder diverticula in the oldest individual (subject 1) were suggestive of a copper metabolism defect.[34] In subject 1, a persistent severe reduction of serum copper levels was documented, and urinary copper excretion over 24 h and serum ceruloplasmin level were on the lower range (Table S2). In this subject, exome sequencing did not show presence of pathogenic variants in genes mutated in copper metabolism disorders. However, the hypothesis that the ClC-6 p.Tyr553Cys change interferes with copper metabolism could not be substantiated by the other probands, as no data were available from the deceased subject 2, and no overt copper metabolism abnormalities in blood were observed in subject 3 (Table S2).

Structural Considerations for the p.Tyr553Cys Change in ClC-6

Tyr^{553} is located in a conserved region within the transmembrane part of the transporter (Figure 2B). Tyrosine at this position is conserved in all mammalian CLC Cl^-/H^+-exchangers but is replaced by histidine in algal cmClC and all mammalian CLC Cl^- channels (Figure 2A). Figures 2B and 2C show the position of the equivalent tyrosine in ClC-7, the closest homolog of ClC-6 for which cryo-EM structures are currently available.[32,35] This residue is located in the outward loop between helices P and Q and is distant from the ion translocation pathway as indicated by the position of the "gating glutamate" in Figures 2B and 2C. Motions of this loop region have been implicated in the function of the *E. coli* transporter ecCLC.[36,37] The predicted position of Tyr^{553} is close to the subunit interface of the dimer, which plays a role in the common gating of both subunits of CLC channels and transporters.[38–40] The formation of disulfide bonds between two Cys^{553}-containing subunits of a ClC-6 dimer is not allowed by their distance. However, it can currently not be excluded that the newly introduced Cys^{553} reacts with either Cys^{319} or Cys^{326} on the same subunit.

Impact of p.Tyr553Cys on ClC-6 Ion Transport Properties

To characterize the ion transport properties of the p.Tyr553Cys ClC-6 mutant (ClC-$6^{Tyr553Cys}$), we used a construct in which GFP was fused to the ClC-6 N terminus. GFP-ClC-6 fusion proteins are partially mistargeted to the plasma membrane where they can be studied electrophysiologically as shown in our previous work[22] which included an analysis of the uncoupling p.Glu200Ala mutant later found to be associated with epilepsy.[24,25] Whole cell patch-clamp analysis of transfected CHO cells using ionic conditions that suppress cation currents showed that both WT and p.Tyr553Cys mutant ClC-6 gave strongly outwardly rectifying currents that were above background only for voltages > +60 mV (Figure 3A). Compared to the currents measured in cells transfected with the WT protein, which appeared almost instantaneously upon depolarization as described,[22] ClC-$6^{Tyr553Cys}$-associated currents activated slowly with time course in the range of a second (Figure 3A) and reached larger steady-state amplitudes (Figures 3B and 3C). Currents were reduced when extracellular chloride was almost completely replaced by iodide (Figure 3A), in line with the ion selectivity of ClC-6 and CLC channels and transporters in general.[9,22] In contrast to currents elicited by WT ClC-6,[22] ClC-4 and ClC-5,[41] or ClC-7,[39] which all decrease with acidic extracellular pH (pH_o), currents of ClC-$6^{Tyr553Cys}$ were insensitive to pH_o between pH 8.5 and 5.5 (Figures 3D and 3E). Hence the activity of the ClC-$6^{Tyr553Cys}$ mutant is not expected to decrease at the acidic pH of late endosomes, further increasing the gain-of-function in its native environment.

Expression of p.Tyr553Cys ClC-6 Mutant Generates Giant LAMP1-Positive Vacuoles

Agreeing with the native intracellular localization of ClC-6 in brain,[21] immunofluorescence of HeLa cells transfected with WT ClC-6 revealed small cytoplasmic vesicles that were in part co-labeled with LAMP1, a marker for late endosomes and lysosomes (Figure 4A). Immunolabeling of transfected GFP-ClC-6 with anti-GFP antibodies yielded similar results in addition to faint plasma membrane staining caused by the partial mislocalization of ClC-6 by the N-terminal tag. Transfection of ClC-$6^{Tyr553Cys}$ led to conspicuously enlarged vesicles (Figure 4B) that often reached diameters of >2 μm and filled a large part of the cytoplasm. We used live cell imaging of U2OS human osteosarcoma knock-in cells engineered to express a LAMP1-GFP fusion protein[28] to follow the effect of ClC-$6^{Tyr553Cys}$ transfection on LAMP1-positive structures (Video S1). The diameter of LAMP1-positive vesicles increased more than 10-fold over a period of more than 10 h after transfection, apparently largely by vesicular fusion events as observed with fusion of giant vesicles (Video S2, Figure 4G). Eventually, almost the entire cytoplasm was filled with abnormal spherical structures. Their membranes were labeled for both ClC-6 and LAMP1 (Figure 4B), suggesting a late endosomal-lysosomal origin. We also analyzed the effect of the ClC-$6^{Glu200Ala}$ mutant that had been associated with the clinical diagnosis of infantile spasm or West syndrome.[24,25] ClC-$6^{Glu200Ala}$ overexpression produced moderately enlarged LAMP1-positive vesicles (Figure 4C) that reached on average about half the diameter of those generated by ClC-$6^{Tyr553Cys}$. In ClC-$6^{Glu200Ala}$ overexpressing cells, the average diameter of LAMP1-positive compartments was roughly 3-fold larger than in WT ClC-6 transfected cells.

Ion Transport of ClC-$6^{Tyr553Cys}$ and H^+-ATPase Activity Are Required for Vacuole Generation

The formation of large, round vesicles requires the addition of membrane by vesicle fusion as well as an influx

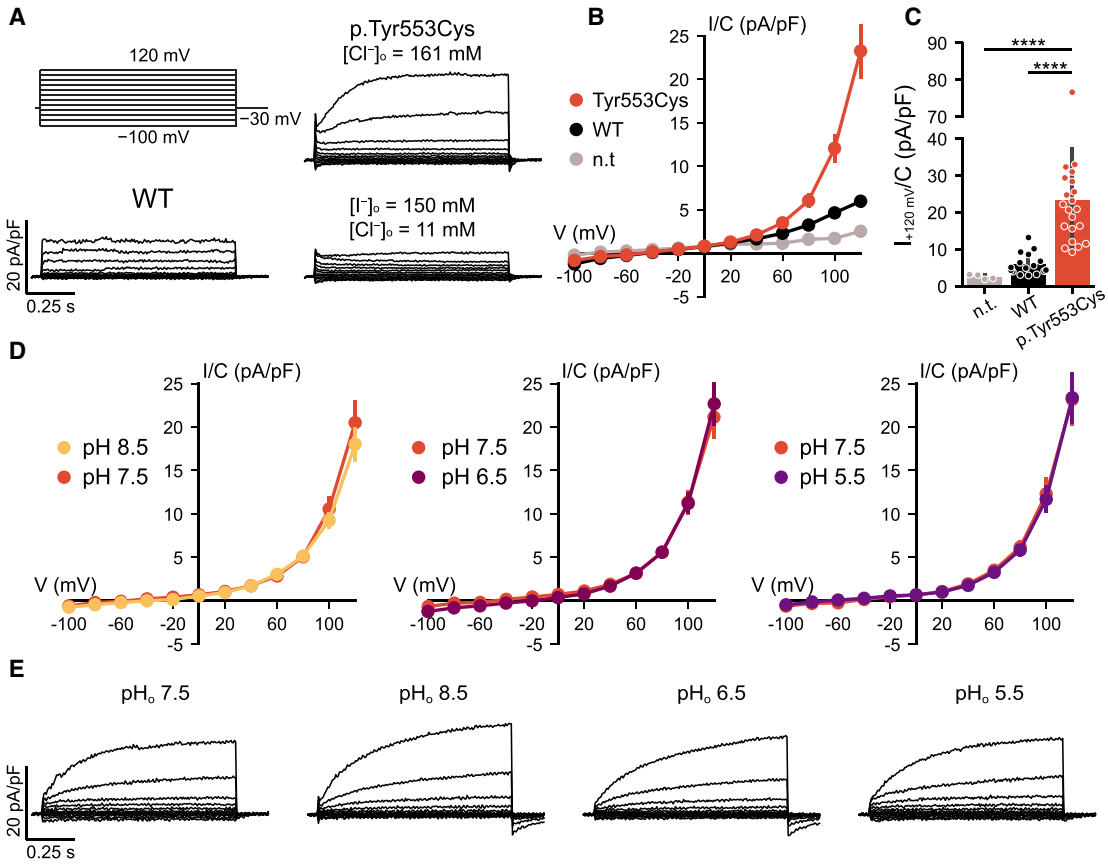

Figure 3. Electrophysiological Analysis of WT and p.Tyr553Cys Mutant ClC-6

(A) Voltage clamp protocol (top left) and example traces obtained from CHO-K1 cells transfected with WT (bottom left) or p.Tyr553Cys mutant ClC-6 in Cl^--containing bath solution (top right) and p.Tyr553Cys ClC-6 in I^--containing bath solution (bottom right).

(B) Current-voltage relationship of steady-state current (assessed at the end of each 1 s step) in non-transfected cells (n.t.) and cells transfected with GFP-ClC-6 (WT) or GFP-ClC-$6^{Tyr553Cys}$ (p.Tyr553Cys).

(C) Steady-state current density at +120 mV.

(D) Current-voltage relationship of steady-state current of GFP-ClC-$6^{Tyr553Cys}$ recorded at different external pH (pH_o).

(E) Example traces obtained from GFP-ClC-$6^{Tyr553Cys}$ at pH_o of 7.5 (equivalent to the traces in A), 5.5, 6.5, and 8.5, obtained from the same cell.

****$p < 0.0001$ (Dunn's post hoc test after Kruskal-Wallis test; p values are corrected using the Benjamini-Hochberg procedure). Error bars, SD (C); SEM (B, D).

of fluid. Water transport across biological membranes requires osmotic gradients which are mostly generated by differences in ion concentrations. We therefore asked whether the generation of large vacuoles by ClC-$6^{Tyr553Cys}$ requires ion transport through ClC-6. We first generated a ClC-6 double mutant in which the p.Tyr553Cys variant was combined with the "transport deficient" (*td*) p.Glu267Ala substitution that affects the cytoplasmic "proton glutamate."[33] Neutralization of this glutamate abolishes both Cl^-- and H^+-transport in ClC-6[22] and other mammalian CLC exchangers.[39,42,43] Transfection of ClC-$6^{Glu267Ala/Tyr553Cys}$ failed to generate large vesicles (Figure 4D), revealing an absolute dependence on ClC-6 ion transport. We next asked whether the formation of those vesicles requires Cl^- transport, but not Cl^-/H^+-exchange, and generated a ClC-$6^{Glu200Ala/Tyr553Cys}$ double mutant. The p.Glu200Ala substitution (*unc* for uncoupled) in the "gating glutamate" selectively abolishes transport of H^+ and converts ClC-6[22] and other CLCs[39,44–46] into pure, pH-independent Cl^- conductors that almost lack voltage dependence. Transfection of ClC-$6^{Glu200Ala/Tyr553Cys}$ led to mildly enlarged vesicles (Figure 4E) in the same size range as observed with ClC-$6^{Glu200Ala}$ expression (Figure 4C). Hence the full impact of the p.Tyr553Cys mutant on vesicle size requires Cl^-/H^+-coupling or, less likely, the slow voltage-dependent gating of ClC-$6^{Tyr553Cys}$ that is lost in uncoupling *unc* mutants. Ion transport across membranes of endosomes and lysosomes is energized by V-type H^+-ATPases. Inhibition of the proton pump by bafilomycin abolished vacuole enlargement by ClC-$6^{Tyr553Cys}$ (Figure S1). Importantly, it also led to the shrinkage of ClC-$6^{Tyr553Cys}$-enlarged vacuoles after acute addition (Video S3; Figure S1C). Hence the generation and maintenance of large vesicles requires H^+-ATPase-driven $2Cl^-/H^+$-exchange of ClC-$6^{Tyr553Cys}$.

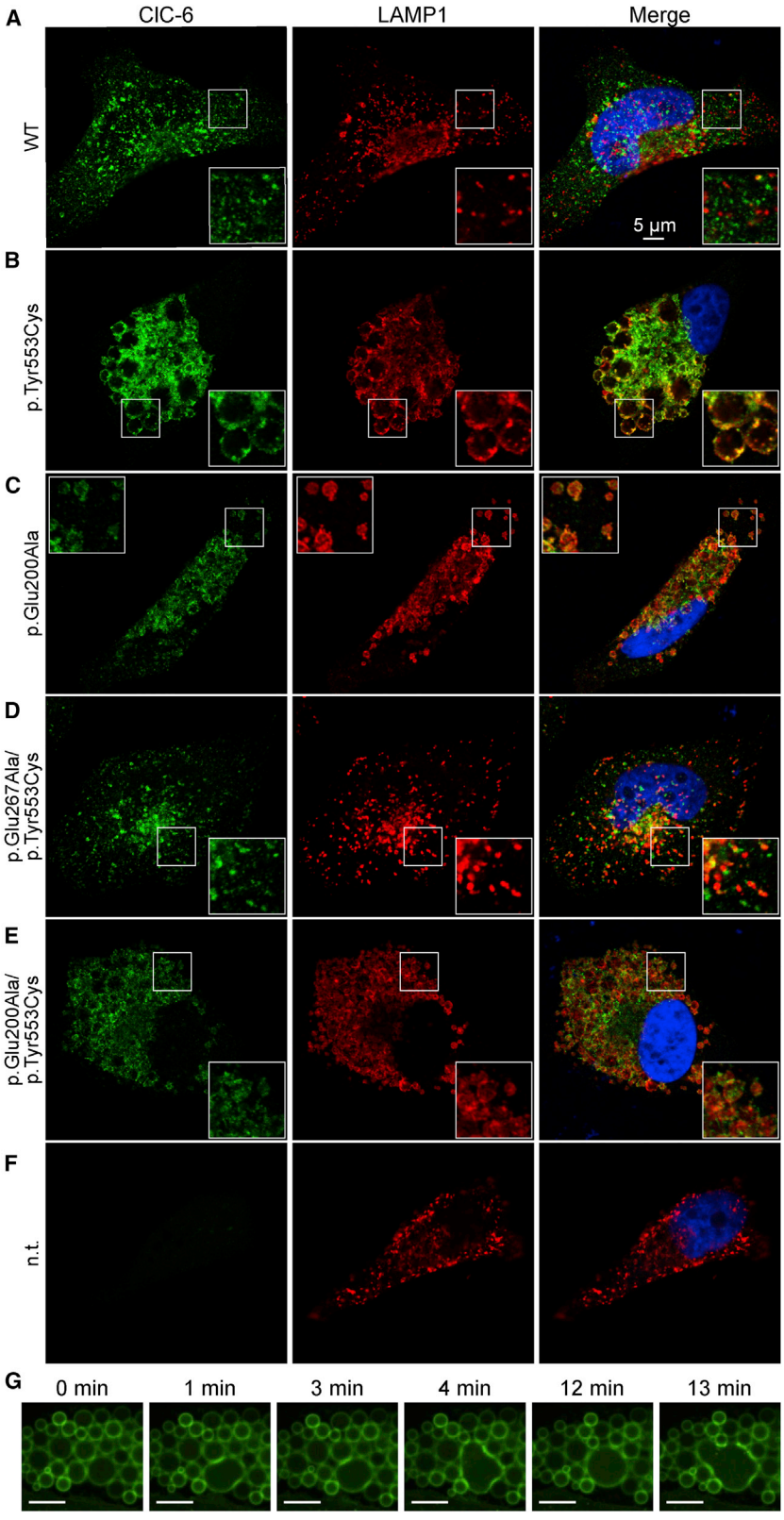

Figure 4. Generation of Large LAMP1-Positive Vacuoles by ClC-6 Mutants

(A–F) HeLa cells were transfected with (A) WT ClC-6, (B) ClC-$6^{Tyr553Cys}$, (C) ClC-$6^{Glu200Ala}$, (D) ClC-$6^{Glu267Ala/Tyr553Cys}$, (E) ClC-$6^{Glu200Ala/Tyr553Cys}$, or (F) not transfected (control). Cells were immunolabeled for ClC-6 (left panels) and the late endosomal/lysosomal marker protein LAMP1 (middle panels). Right panels show the overlayed signals. Giant LAMP1-positive vesicles were generated by the p.Tyr553Cys (B), and moderately enlarged vesicles by the *unc* p.Glu200Ala mutant (C). Insertion of the ion transport blocking p.Glu267Ala *td* substitution abolished the effect of p.Tyr553Cys (D), whereas the *unc* p.Glu200Ala substitution reduced the effect of p.Tyr553Cys to that seen with p.Glu200Ala alone (C, E).

(G) Selected frames from a live-cell imaging video (Video S2) showing fusion of giant vesicles in U2OS LAMP1-GFP cells transfected with ClC-$6^{Tyr553Cys}$. Scale bar, 10 μm.

Abnormally Enlarged Vacuoles Are Less Acidified and Only Partially Accessible to Endocytic Cargo

Labeling acidic compartments of U2OS LAMP1-GFP cells with LysoTracker (Figure 5A) showed that roughly half of the normal-sized LAMP1-positive structures of WT ClC-6-transfected cells were acidified. Since LAMP1 is a marker for both late endosomes and lysosomes, this pattern is compatible with only strongly acidic lysosomes being labeled. In cells transfected with ClC-$6^{Tyr553Cys}$ (Figure 5A), only a fraction of enlarged LAMP1-positive vacuoles displayed uniform LysoTracker fluorescence. To confirm these results, we co-transfected HeLa cells with mCherry-ClC-6 and CD63-phluorin,[47] which is targeted to lysosomal compartments and positions pH-sensitive phluorin into their lumina. Phluorin fluorescence, which is quenched by acidic pH, was not observed in mCherry-ClC-6^{WT} transfected cells, but in cells co-transfected with mCherry-ClC-$6^{Tyr553Cys}$, where it faintly labeled the membranes of mCherry-positive vesicles (Figure S2). Hence many, if not most, of the largest ClC-$6^{Tyr553Cys}$-generated vesicles are only poorly acidified.

To quantify luminal pH, we loaded vesicles with OregonGreen 488 dextran, a ratiometric pH-sensitive dye, by endocytic uptake and subsequent chase. The pH of those vesicles that had accumulated the dextran-coupled dye was quantified. Vesicles of ClC-$6^{Tyr553Cys}$ transfected cells (pH_{lum} = 5.8 ± 0.4) was significantly less acidic compared to ClC-6^{WT} transfected cells (pH_{lum} = 4.5 ± 0.5) (Figure S3). Unlike membrane-permeable LysoTracker, dextran-coupled indicators report pH only of those vesicles that have accumulated dye after

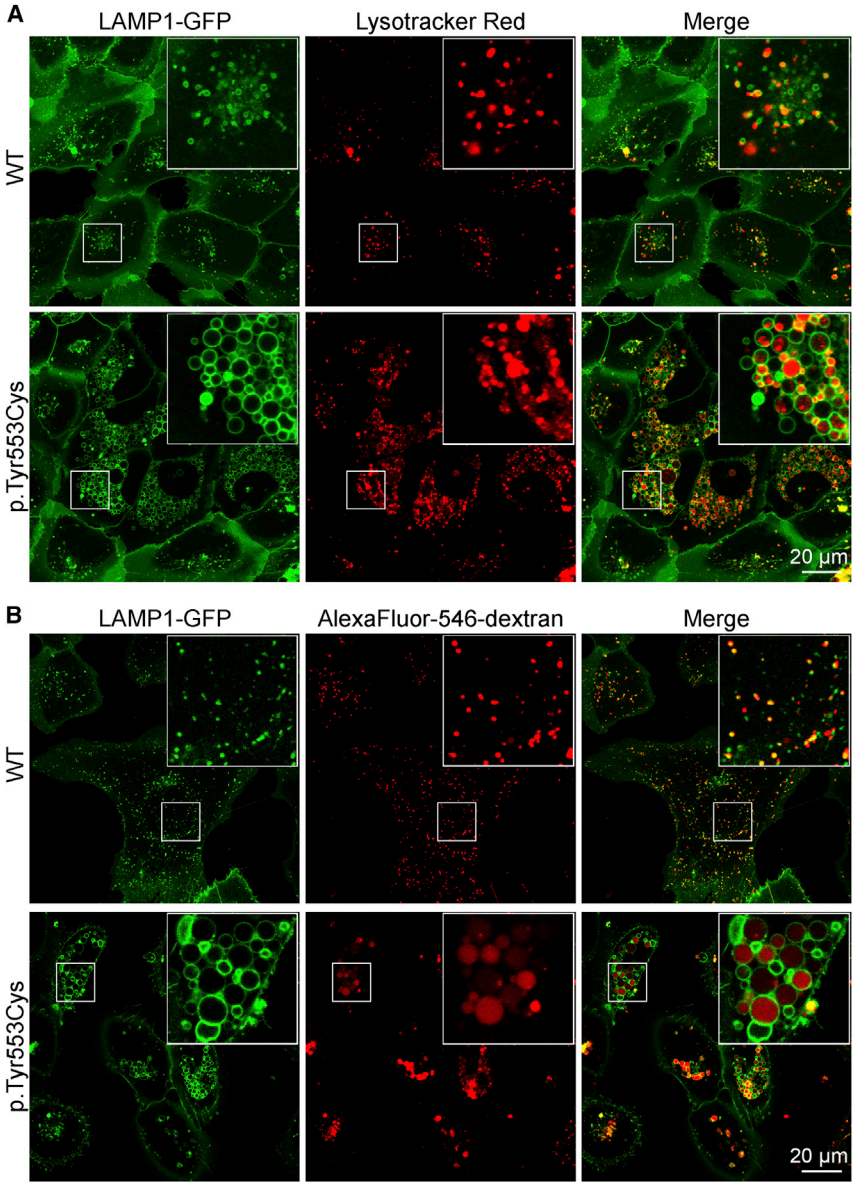

Figure 5. Vacuoles Formed by ClC-6^{Tyr553Cys} Show Variable Acidification and Accessibility to Endocytic Cargo

U2OS LAMP1-GFP cells transfected with either WT or p.Tyr553Cys mutant ClC-6 as indicated.

(A) LysoTracker Red staining of acidic compartments reveals that many LAMP1-GFP-expressing vesicles lack significant acidification (n = 3 independent experiments).

(B) Cells labeled with pH-insensitive Alexa Fluor-546 dextran by endocytosis and a subsequent 2 h chase. Endocytosed fluorescently labeled dextran labels the entire lumen of some vesicles, whereas others are devoid of dextran or show fluorescent spots in their lumen, possibly indicating multivesicular bodies. Similar spots within some giant vesicles are also seen with LysoTracker labeling in (A).

endocytosis. Uptake of Alexa Fluor-546 dextran, which displays pH-independent fluorescence, revealed that only part of the large LAMP1- and ClC-6^{Tyr553Cys}-positive vacuoles efficiently accumulated the dye (Figures 5B and S4). On average, these vesicles seemed to have larger diameters than those labeled by LysoTracker dyes. Oregon-Green dextran and LysoTracker may report luminal pH in different, partially overlapping compartments.

While being positive for LAMP1 and CD63, the large ClC-6^{Tyr553Cys}-generated and ClC-6-expressing vacuoles lacked other typical characteristics of lysosomes such as $pH_{lum} < 5.0$ and easy accessibility by endocytic cargo. They also lacked the lysosomal enzyme cathepsin D, which partially co-localized with ClC-6^{WT}- and ClC-6^{Glu200Ala}-transfected cells (Figure S5). While these properties may fit to late endosomes, the predominant site of native ClC-6 expression,[21] the large ClC-6^{Tyr553Cys}-generated vacuoles are clearly pathological and probably interfere with various cellular functions.

Fibroblasts from Affected Individuals Lack Enlarged Vacuoles

Fibroblasts were derived from subjects 1 and 3 and stained for LAMP1 and cathepsin D in comparison to control fibroblasts (Figure S6A). In contrast to HeLa or U2OS cells overexpressing mutant ClC-6^{Tyr553Cys} (Figures 4 and 5), no obvious difference in the number and size of labeled structures was found. Both in control subject and affected subject fibroblasts, we observed some cell-to-cell variability in the size of LAMP1-positive structures, as shown in the two examples of control fibroblasts (Figure S6A). Likewise, imaging acidic intracellular compartments with LysoTracker or LysoSensor failed to reveal differences between fibroblasts from affected individuals and control subjects (Figure S6B). The apparent discrepancy of these finding with those obtained using transfected cells as experimental system may be attributed to differences in protein levels, not only because transfection leads to overexpression, but because the ClC-6 protein is primarily found in neuronal tissue.[21] Indeed, western blot analysis of mouse tissues (Figure S7) showed that the ClC-6 protein was prominently present in brain, but barely detectable or absent in fibroblasts and intestine.

Discussion

ClC-6 is a Cl^-/H^+ exchanger that is predominantly found on late endosomes.[21] Disruption of *Clcn6* in mice causes

mild lysosomal storage disease,[21] but as yet convincing evidence that *CLCN6* mutations underlie human disease has been lacking. We report here the identification of the same *de novo CLCN6* mutation, c.1658A>G (p.Tyr553Cys), in three unrelated individuals with a consistent early-onset neurodegenerative disorder. The missense mutation profoundly changes ClC-6 ion transport properties, resulting in a gain of currents that is especially prominent at acidic external (luminal) pH as found in late endosomes and lysosomes. The *CLCN6* missense variant p.Tyr553Cys was associated with a severe clinical course, including pronounced developmental delay, lack of motor development, chronic respiratory insufficiency, and brainstem lesions in all subjects, as well as cortical atrophy, neurogenic bladder, and peripheral sensory neuropathy in two subjects. Remarkably, MRI scans in all subjects revealed bilateral restriction diffusion in cerebral peduncles and dorsal brainstem and/or midbrain that are rare brain imaging findings. Together with our functional evaluation of another *de novo CLCN6* missense variant, p.Glu200Ala, previously reported in association with early infantile epileptic encephalopathy,[24,25] our findings firmly establish *CLCN6* as a gene implicated in neurological conditions, when mutated.

ClC-6 is one of the least explored mammalian members of the CLC family. Whereas the *Clcn6* mRNA is widely expressed across tissues,[20,48] the ClC-6 protein rather appears restricted to the nervous system[21] where it localizes to late endosomes as indicated by partial co-localization with LAMP1.[21] ClC-6 expression partially overlaps with that of lysosomal ClC-7, whose disruption causes neurodegeneration and pronounced lysosomal storage disease in brain and kidney,[49,50] as well as osteopetrosis.[17] By contrast, *Clcn6*$^{-/-}$ mice only have mild lysosomal storage[21] associated with slight, late neurodegeneration,[23] nonspecific cognitive problems, and reduced pain perception.[21] The latter symptom, which also occurred in subject 1, might be due to the accumulation of storage material in dorsal root ganglia neurons.[21]

Previous screening of 75 individuals with mild neuronal ceroid lipofuscinosis for *CLCN6* mutations yielded two heterozygous missense variants whose pathogenicity remained unclear.[21] *CLCN6* coding variants were also found in subjects with infantile epilepsy,[51] but their pathogenicity remained doubtful as no effects on ClC-6 currents were observed.[51] The *de novo CLCN6* variant c.533A>C (p.Glu178Ala) (according to GenBank: NM_001256959.1) was identified in a 5-month-old male with microcephaly, developmental delay, and infantile spasms that later changed to tonic-clonic and myoclonic seizures and enlarged subarachnoid space in brain imaging.[24] The same *de novo* missense variant has been described in an individual with West syndrome, suggesting that this variant is associated with early infantile epileptic encephalopathy.[25] Description of the reported variant c.533A>C (p.Glu178Ala) in the commonly used *CLCN6* transcript variant 1, GenBank: NM_001286.4: c.599A>C (p.Glu200Ala), revealed that this substitution affects the critical gating glutamate[12] that had been functionally studied previously in ClC-6.[22] This pore glutamate is crucial for anion/proton exchange, as first shown for bacterial ecClC.[44] Like gating glutamate mutations in other mammalian CLC exchangers,[39,45,46,52] p.Glu200Ala converts the strongly voltage-dependent Cl^-/H^+-exchange of ClC-6 into an uncoupled, ohmic Cl^- conductance that is no longer inhibited by extracellular (topologically equivalent to vesicle-inside) acidic pH.[22] The fact that similar uncoupling mutations in other CLC exchangers lead to disease in mice[53–55] and humans[56,57] suggest that the p.Glu200Ala change is pathogenic, as now supported by the observation of enlarged vesicles upon ClC-6^{Glu200Ala} expression in HeLa cells. However, unlike individuals who carry the *CLCN6* p.Glu200Ala substitution in a heterozygous state,[24,25] mice heterozygous for similar uncoupling *Clcn3* or *Clcn7* mutations lack obvious abnormalities.[54,55] The p.Glu200Ala variant in ClC-6 was associated with early-onset epileptic encephalopathy.[24,25] In contrast, the three individuals carrying the p.Tyr553Cys substitution described here did not show epilepsy, with the possible exception of subject 1 who may have had epileptic episodes at 4 years of age. Whereas the p.Glu200Ala change is associated with spasms,[24] the three subjects with the p.Tyr553Cys substitution rather displayed severe hypotonia and chronic respiratory insufficiency as prominent common symptoms.

Subject 1 had severely decreased serum copper levels, low urinary copper excretion, and abnormal copper content in hair, features overlapping those occurring in Menkes disease (MIM: 309400).[58,59] We could not determine serum copper in subject 2, and serum copper concentrations were normal in subject 3. Of note, serum copper levels can be in the low-normal range in infants affected by Wilson and Menkes diseases.[34,60] Intriguingly, ablation of the *S. cerevisiae* CLC protein Gef1p impairs copper-loading of the iron transporter Fet3p,[61] and the resulting iron-suppressible growth phenotype can be rescued by other CLCs including ClC-6.[48,62] However, Gef1p localizes to the Golgi,[63] which in mammals contains the bulk of ATP7A, whereas ClC-6 resides in late endosomes and seems restricted to brain.[21] We also measured serum copper levels in *Clcn6*$^{-/-}$ mice.[21] They overlapped with those of control animals (359 ± 26 μg/mL versus 381 ± 22 μg/mL; $p = 0.1$, Mann-Whitney U-test).[64] Without further support for role of ClC-6^{Tyr553Cys} in copper metabolism by animal models or larger cohorts of patients, these observations rather argue against this hypothesis.

Tyr553 is located in a luminal loop, while Glu200 is located in the center of the pore. Hence both the p.Tyr553Cys and p.Glu200Ala mutations are unlikely to change the localization of ClC-6 by affecting interactions with the sorting machinery. The p.Tyr553Cys substitution altered several aspects of ClC-6 ion transport. It strongly slowed the depolarization-induced activation of ClC-6

which normally opens almost instantaneously, revealing that ClC-6 is a voltage-gated transporter like ClC-7 which needs several seconds to open.[39] The localization of Tyr^{553} at the interface of both subunits is compatible with a role in the common gating process that acts on both subunits of CLC channels and transporters.[38–40] The abnormal slow activation of ClC-6 reduces current amplitudes shortly after depolarization, in intriguing contrast to several *CLCN7* mutations in dominant osteopetrosis, which accelerate the voltage-induced activation of ClC-7.[39] In contrast, the increase of steady-state currents, combined with a loss of pH-dependence, represent a clear gain-of-function of the p.Tyr553Cys mutant, a change that most likely underlies the severe clinical course in all three subjects. Whereas the increasingly acidic pH along the endolysosomal pathway would progressively reduce the activity of WT ClC-6, possibly in a negative feedback loop to control luminal acidification,[41] both ClC-6 p.Glu200Ala and p.Tyr553Cys mutants would retain their unabated transport activity in late endosomes and lysosomes. Unlike ClC-$6^{Tyr553Cys}$, however, ClC-$6^{Glu200Ala}$ has additionally lost both its voltage dependence and proton coupling. Hence, it is not surprising that the two *CLCN6* mutations are associated with different neurological phenotypes.

Phenotypes observed with a loss of vesicular CLC exchangers were initially attributed to impaired acidification of endolysosomes caused by a lack of neutralizing currents for vesicular H^+-ATPases.[17,65] Whereas the acidification of renal endosomes from *Clcn5*$^{-/-}$ mice is indeed reduced,[53,66] *Clcn7*$^{-/-}$ lysosomes have normal steady-state pH[49,54] but show substantially reduced luminal Cl^- concentration,[54] suggesting an important role for lysosomal Cl^-.[3,54,67,68] This notion is further supported by knock-in mice and affected individuals in which the Cl^-/H^+-exchange of ClC-3, ClC-5, or ClC-7 is converted into an uncoupled Cl^- conductance by point mutations.[53–56] While not supporting a role of ClC-6 in luminal acidification, our work suggests that ClC-6 accumulates Cl^- into vesicles, at least when carrying the p.Tyr553Cys or the p.Glu200Ala mutation.

ClC-$6^{Tyr553Cys}$, and to a minor degree ClC-$6^{Glu200Ala}$, induced the enlargement of intracellular vesicles upon overexpression. This situation is not unprecedented. Overexpression of an N-terminal splice variant of ClC-3 generates LAMP1-positive vacuoles in CHO and Huh-7 cells.[69] These vesicles are positive for LAMP1 and LAMP2, contain cathepsin D, are acidified, and, like the vacuoles described here, depend on the activity of the proton pump and on $2Cl^-/H^+$-exchange. Large cytoplasmic vacuoles were also observed with the *CLCN7* p.Tyr517Cys variant that was found *de novo* in patients with lysosomal storage disease and albinism.[70] These vacuoles were present in transfected cells, subject fibroblasts, and knock-in mice. While lysosomes appeared more acidic in cells with ClC-$7^{Tyr715Cys}$, the large cytoplasmic vacuoles were not acidified.[70] The p.Tyr715Cys exchange increases ClC-7 currents about 3-fold without changing its slow activation by depolarization. It is not clear whether it abolishes inhibition by acidic pH as found here for ClC-$6^{Tyr553Cys}$.

Like vesicles generated by ClC-3 or ClC-$7^{Tyr715Cys}$, ClC-$6^{Tyr553Cys}$-elicited vacuoles were LAMP1 positive. They resembled ClC-$7^{Tyr715Cys}$-, but not ClC-3-generated vacuoles, in not being strongly acidified.[69,70] Their generation required ion transport activity of ClC-$6^{Tyr553Cys}$. Bona fide complete disruption of ion transport by the p.Glu267Ala mutation abolished the effect of ClC-$6^{Tyr553Cys}$ on vesicle size. Reminiscent of the disruption of ClC-3-induced vacuole formation by an *unc* mutation,[69] the uncoupling p.Glu200Ala substitution severely reduced, albeit did not abolish, vacuole generation with the ClC-$6^{Glu200Ala/Tyr553Cys}$ double mutant. Model calculations suggest that vesicles acidified by proton pumps may reach more acidic pH and accumulate much more Cl^- in the presence of $2Cl^-/H^+$-exchangers (embodied by CLCs) rather than Cl^- channels (as generated by CLC *unc* mutants).[54] Indeed, luminal Cl^- concentrations were markedly reduced in *Clcn7*$^{unc/unc}$ lysosomes.[54] Even though most of the large ClC-$6^{Tyr553Cys}$ vacuoles were only poorly acidified, the inhibition of vacuole formation and the shrinkage of preformed vacuoles by the H^+-ATPase inhibitor bafilomycin suggests that a pH gradient drives Cl^-/H^+-exchange-mediated Cl^- accumulation and subsequent water influx. However, osmotic swelling is not sufficient to explain the generation of vacuoles since they need to substantially increase their limiting membranes. This requires an imbalance between membrane fusion and fission, which in turn might be modulated by osmotic pressure. Indeed, osmotic shrinkage has been implicated in the resolution of macropinosomes, phagosomes, and autolysosomes.[71] Loss of luminal Na^+ and Cl^- leads to shrinkage-induced generation of membrane protrusions, which can bind BAR domain-containing proteins that induce membrane tubulation and finally fission of small vesicles.[72] Hence an increase in luminal osmotic pressure by ClC-$6^{Tyr553Cys}$ might inhibit membrane fission and thereby enlarge vesicles. In addition, there might be an effect on membrane fusion, as suggested by live-cell imaging showing that the largest vesicles arise from fusion of already enlarged vesicles. The observation that these newly fused vesicles soon acquire a round shapes implies that they rapidly take up salt and water after membrane fusion.

The ClC-6 mutants might affect vesicle size also by non-osmotic effects of changed endolysosomal ion concentrations or altered membrane voltage.[3] Luminal pH can affect vesicle budding, fusion, and trafficking, and luminal Cl^- concentration has important, though poorly understood roles.[3,54,55,67,68] Although only Cl^- and H^+ are directly transported by vesicular CLCs, CLC transport activity may change luminal concentrations of other ions including Ca^{2+}.[68] The crucial role of lysosomes in cellular metabolism and the multitude of trafficking events between various intracellular compartments further complicate the picture. Mouse models and new insights from human diseases, such as the present findings, suggest

that ion transport across endosomal and lysosomal membranes must be finely tuned. We are still far from integrating the various channels, transporters, and other proteins of endosomes and lysosomes in a comprehensive, consistent model.

The lack of conspicuously enlarged lysosome-like vacuoles in fibroblasts of subjects 1 and 3 is not surprising because the ClC-6 protein, unlike ClC-7, is mainly expressed in neurons[21] (Figure S7). Accordingly *Clcn6*$^{-/-}$ mice,[21] the individuals reported here, and subjects carrying the p.Glu200Ala substitution,[24,25] have neurological disorders with clinical features depending on the specific biophysical changes provoked by the mutation. We speculate that the p.Tyr553Cys change may cause, in addition to enlarged cytoplasmic vacuoles, lysosomal storage disease in neurons of affected individuals. These postmitotic cells particularly depend on the elimination of potentially toxic intracellular proteins and aggregates.

Our work establishes that different gain-of-function mutations in *CLCN6* can underlie distinct, predominantly neurological phenotypes. Whereas the *de novo* p.Glu200Ala substitution is associated with a hyperexcitability phenotype, the three subjects with the *de novo* p.Tyr553Cys variant have an early-onset neurodegenerative disorder comprising global developmental delay, absent motor development, and chronic respiratory insufficiency as common, and cortical atrophy, neurogenic bladder, and peripheral sensory neuropathy as variable features. Notably, they lack seizures as a main sign. We believe that the specific combination of clinical features together with the rare MRI signal abnormalities in cerebral peduncles and surrounding brain regions makes the *CLCN6* p.Tyr553Cys-associated disorder recognizable and allows a clinical diagnosis. Together with observations that different bona fide gain-of-function mutations in *CLCN7* cause phenotypes that only partially overlap with those observed with a loss of ClC-7,[17,39,70] the present work challenges our efforts to understand how specific alterations in endosomal/lysosomal ion transport lead to diverse phenotypes at the cellular and organismal levels.

Data and Code Availability

The pathogenic variant identified in this work has been submitted to ClinVar (SCV001426224). WES datasets have not been deposited in a public repository due to privacy and ethical restrictions but are available from the corresponding authors on request.

Supplemental Data

Supplemental Data can be found online at https://doi.org/10.1016/j.ajhg.2020.11.004.

Acknowledgments

We thank the families for their participation in this study, Malik Alawi for bioinformatics analysis, Martin Lehmann for help with live cell imaging, Inka Jantke, Carolin Backhaus, Janet Liebold, and Muhammad Kabbani for skillful technical assistance, and Carlo Dionisi Vici for discussions. We thank Ian Ganley (Dundee) for U2OS LAMP1-GFP cells and Christian Rosenmund (Berlin) for CD63-phluorin. F.L.H. was supported by the Research Promotion Fund of the Faculty of Medicine (FFM) of the University Medical Center Hamburg-Eppendorf. This work was supported, in part, by grants from the Deutsche Forschungsgemeinschaft (FOR 2652 (Je164/14-1) and Exc257 "Neurocure" to T.J.J., and KU 1240/10-1 to K.K.) and the Prix Louis-Jeantet de Médecine to T.J.J., Fondazione Bambino Gesù (Vite Coraggiose) and Italian Ministry of Health (CCR-2017-23669081) to M.T., and the Children's Discovery Institute of Washington University and St. Louis Children's Hospital and the National Human Genome Research Institute (U01 HG010215) to F.S.C. The content is solely the responsibility of the authors and does not necessarily represent the official views of the National Institutes of Health.

Declaration of Interests

All the authors declare no competing interests.

Received: August 21, 2020
Accepted: November 2, 2020
Published: November 19, 2020

Web Resources

ANNOVAR, http://annovar.openbioinformatics.org/en/latest/
ClinVar, https://www.ncbi.nlm.nih.gov/clinvar/
dbNSFP v.2.0, https://sites.google.com/site/jpopgen/dbNSFP
ExAC Browser, http://exac.broadinstitute.org/
gnomAD Browser, https://gnomad.broadinstitute.org/
InterVar, http://wintervar.wglab.org
OMIM, https://www.omim.org/
RCSB Protein Data Bank, http://www.rcsb.org/pdb/home/home.do

References

1. Dautry-Varsat, A., Ciechanover, A., and Lodish, H.F. (1983). pH and the recycling of transferrin during receptor-mediated endocytosis. Proc. Natl. Acad. Sci. USA *80*, 2258–2262.
2. Morgan, A.J., Platt, F.M., Lloyd-Evans, E., and Galione, A. (2011). Molecular mechanisms of endolysosomal Ca^{2+} signalling in health and disease. Biochem. J. *439*, 349–374.
3. Scott, C.C., and Gruenberg, J. (2011). Ion flux and the function of endosomes and lysosomes: pH is just the start: the flux of ions across endosomal membranes influences endosome function not only through regulation of the luminal pH. BioEssays *33*, 103–110.
4. Lakpa, K.L., Halcrow, P.W., Chen, X., and Geiger, J.D. (2020). Readily Releasable Stores of Calcium in Neuronal Endolysosomes: Physiological and Pathophysiological Relevance. Adv. Exp. Med. Biol. *1131*, 681–697.
5. Anne, C., and Gasnier, B. (2014). Vesicular neurotransmitter transporters: mechanistic aspects. Curr. Top. Membr. *73*, 149–174.
6. Xu, H., Martinoia, E., and Szabò, I. (2015). Organellar channels and transporters. Cell Calcium *58*, 1–10.

7. Jentsch, T.J. (2015). Discovery of CLC transport proteins: cloning, structure, function and pathophysiology. J. Physiol. *593*, 4091–4109.
8. Huizing, M., and Gahl, W.A. (2020). Inherited disorders of lysosomal membrane transporters. Biochim Biophys Acta Biomembr *1862*, 183336.
9. Jentsch, T.J., and Pusch, M. (2018). CLC Chloride Channels and Transporters: Structure, Function, Physiology, and Disease. Physiol. Rev. *98*, 1493–1590.
10. Ludewig, U., Pusch, M., and Jentsch, T.J. (1996). Two physically distinct pores in the dimeric ClC-0 chloride channel. Nature *383*, 340–343.
11. Middleton, R.E., Pheasant, D.J., and Miller, C. (1996). Homodimeric architecture of a ClC-type chloride ion channel. Nature *383*, 337–340.
12. Dutzler, R., Campbell, E.B., Cadene, M., Chait, B.T., and MacKinnon, R. (2002). X-ray structure of a ClC chloride channel at 3.0 Å reveals the molecular basis of anion selectivity. Nature *415*, 287–294.
13. Lloyd, S.E., Pearce, S.H., Fisher, S.E., Steinmeyer, K., Schwappach, B., Scheinman, S.J., Harding, B., Bolino, A., Devoto, M., Goodyer, P., et al. (1996). A common molecular basis for three inherited kidney stone diseases. Nature *379*, 445–449.
14. Piwon, N., Günther, W., Schwake, M., Bösl, M.R., and Jentsch, T.J. (2000). ClC-5 Cl^--channel disruption impairs endocytosis in a mouse model for Dent's disease. Nature *408*, 369–373.
15. Hu, H., Haas, S.A., Chelly, J., Van Esch, H., Raynaud, M., de Brouwer, A.P., Weinert, S., Froyen, G., Frints, S.G., Laumonnier, F., et al. (2016). X-exome sequencing of 405 unresolved families identifies seven novel intellectual disability genes. Mol. Psychiatry *21*, 133–148.
16. Veeramah, K.R., Johnstone, L., Karafet, T.M., Wolf, D., Sprissler, R., Salogiannis, J., Barth-Maron, A., Greenberg, M.E., Stuhlmann, T., Weinert, S., et al. (2013). Exome sequencing reveals new causal mutations in children with epileptic encephalopathies. Epilepsia *54*, 1270–1281.
17. Kornak, U., Kasper, D., Bösl, M.R., Kaiser, E., Schweizer, M., Schulz, A., Friedrich, W., Delling, G., and Jentsch, T.J. (2001). Loss of the ClC-7 chloride channel leads to osteopetrosis in mice and man. Cell *104*, 205–215.
18. Chalhoub, N., Benachenhou, N., Rajapurohitam, V., Pata, M., Ferron, M., Frattini, A., Villa, A., and Vacher, J. (2003). Grey-lethal mutation induces severe malignant autosomal recessive osteopetrosis in mouse and human. Nat. Med. *9*, 399–406.
19. Lange, P.F., Wartosch, L., Jentsch, T.J., and Fuhrmann, J.C. (2006). ClC-7 requires Ostm1 as a β-subunit to support bone resorption and lysosomal function. Nature *440*, 220–223.
20. Brandt, S., and Jentsch, T.J. (1995). ClC-6 and ClC-7 are two novel broadly expressed members of the CLC chloride channel family. FEBS Lett. *377*, 15–20.
21. Poët, M., Kornak, U., Schweizer, M., Zdebik, A.A., Scheel, O., Hoelter, S., Wurst, W., Schmitt, A., Fuhrmann, J.C., Planells-Cases, R., et al. (2006). Lysosomal storage disease upon disruption of the neuronal chloride transport protein ClC-6. Proc. Natl. Acad. Sci. USA *103*, 13854–13859.
22. Neagoe, I., Stauber, T., Fidzinski, P., Bergsdorf, E.Y., and Jentsch, T.J. (2010). The late endosomal ClC-6 mediates proton/chloride countertransport in heterologous plasma membrane expression. J. Biol. Chem. *285*, 21689–21697.
23. Pressey, S.N., O'Donnell, K.J., Stauber, T., Fuhrmann, J.C., Tyynelä, J., Jentsch, T.J., and Cooper, J.D. (2010). Distinct neuropathologic phenotypes after disrupting the chloride transport proteins ClC-6 or ClC-7/Ostm1. J. Neuropathol. Exp. Neurol. *69*, 1228–1246.
24. Wang, Y., Du, X., Bin, R., Yu, S., Xia, Z., Zheng, G., Zhong, J., Zhang, Y., Jiang, Y.H., and Wang, Y. (2017). Genetic Variants Identified from Epilepsy of Unknown Etiology in Chinese Children by Targeted Exome Sequencing. Sci. Rep. *7*, 40319.
25. Peng, J., Wang, Y., He, F., Chen, C., Wu, L.W., Yang, L.F., Ma, Y.P., Zhang, W., Shi, Z.Q., Chen, C., et al. (2018). Novel West syndrome candidate genes in a Chinese cohort. CNS Neurosci. Ther. *24*, 1196–1206.
26. Flex, E., Martinelli, S., Van Dijck, A., Ciolfi, A., Cecchetti, S., Coluzzi, E., Pannone, L., Andreoli, C., Radio, F.C., Pizzi, S., et al. (2019). Aberrant Function of the C-Terminal Tail of HIST1H1E Accelerates Cellular Senescence and Causes Premature Aging. Am. J. Hum. Genet. *105*, 493–508.
27. Kortüm, F., Caputo, V., Bauer, C.K., Stella, L., Ciolfi, A., Alawi, M., Bocchinfuso, G., Flex, E., Paolacci, S., Dentici, M.L., et al. (2015). Mutations in *KCNH1* and *ATP6V1B2* cause Zimmermann-Laband syndrome. Nat. Genet. *47*, 661–667.
28. Munson, M.J., Allen, G.F., Toth, R., Campbell, D.G., Lucocq, J.M., and Ganley, I.G. (2015). mTOR activates the VPS34-UVRAG complex to regulate autolysosomal tubulation and cell survival. EMBO J. *34*, 2272–2290.
29. Steinmeyer, K., Schwappach, B., Bens, M., Vandewalle, A., and Jentsch, T.J. (1995). Cloning and functional expression of rat CLC-5, a chloride channel related to kidney disease. J. Biol. Chem. *270*, 31172–31177.
30. Sobreira, N., Schiettecatte, F., Valle, D., and Hamosh, A. (2015). GeneMatcher: a matching tool for connecting investigators with an interest in the same gene. Hum. Mutat. *36*, 928–930.
31. Burgunder, J.M., Huifang, S., Beguin, P., Baur, R., Eng, C.S., Seet, R.C., Lim, E.C., Ong, B.K., Hunziker, W., and Sigel, E. (2008). Novel chloride channel mutations leading to mild myotonia among Chinese. Neuromuscul. Disord. *18*, 633–640.
32. Schrecker, M., Korobenko, J., and Hite, R.K. (2020). Cryo-EM structure of the lysosomal chloride-proton exchanger CLC-7 in complex with OSTM1. eLife *9*, e59555.
33. Accardi, A., Walden, M., Nguitragool, W., Jayaram, H., Williams, C., and Miller, C. (2005). Separate ion pathways in a Cl^-/H^+ exchanger. J. Gen. Physiol. *126*, 563–570.
34. Kaler, S.G. (2013). Inborn errors of copper metabolism. Handb. Clin. Neurol. *113*, 1745–1754.
35. Zhang, S., Liu, Y., Zhang, B., Zhou, J., Li, T., Liu, Z., Li, Y., and Yang, M. (2020). Molecular insights into the human CLC-7/Ostm1 transporter. Sci. Adv. *6*, b4747.
36. Elvington, S.M., Liu, C.W., and Maduke, M.C. (2009). Substrate-driven conformational changes in ClC-ec1 observed by fluorine NMR. EMBO J. *28*, 3090–3102.
37. Basilio, D., Noack, K., Picollo, A., and Accardi, A. (2014). Conformational changes required for H^+/Cl^- exchange mediated by a CLC transporter. Nat. Struct. Mol. Biol. *21*, 456–463.
38. Duffield, M., Rychkov, G., Bretag, A., and Roberts, M. (2003). Involvement of helices at the dimer interface in ClC-1 common gating. J. Gen. Physiol. *121*, 149–161.
39. Leisle, L., Ludwig, C.F., Wagner, F.A., Jentsch, T.J., and Stauber, T. (2011). ClC-7 is a slowly voltage-gated $2Cl^-/1H^+$-exchanger and requires Ostm1 for transport activity. EMBO J. *30*, 2140–2152.

40. Ludwig, C.F., Ullrich, F., Leisle, L., Stauber, T., and Jentsch, T.J. (2013). Common gating of both CLC transporter subunits underlies voltage-dependent activation of the $2Cl^-/1H^+$ exchanger ClC-7/Ostm1. J. Biol. Chem. *288*, 28611–28619.
41. Friedrich, T., Breiderhoff, T., and Jentsch, T.J. (1999). Mutational analysis demonstrates that ClC-4 and ClC-5 directly mediate plasma membrane currents. J. Biol. Chem. *274*, 896–902.
42. Zdebik, A.A., Zifarelli, G., Bergsdorf, E.-Y., Soliani, P., Scheel, O., Jentsch, T.J., and Pusch, M. (2008). Determinants of anion-proton coupling in mammalian endosomal CLC proteins. J. Biol. Chem. *283*, 4219–4227.
43. Bergsdorf, E.Y., Zdebik, A.A., and Jentsch, T.J. (2009). Residues important for nitrate/proton coupling in plant and mammalian CLC transporters. J. Biol. Chem. *284*, 11184–11193.
44. Accardi, A., and Miller, C. (2004). Secondary active transport mediated by a prokaryotic homologue of ClC Cl^- channels. Nature *427*, 803–807.
45. Scheel, O., Zdebik, A.A., Lourdel, S., and Jentsch, T.J. (2005). Voltage-dependent electrogenic chloride/proton exchange by endosomal CLC proteins. Nature *436*, 424–427.
46. Picollo, A., and Pusch, M. (2005). Chloride/proton antiporter activity of mammalian CLC proteins ClC-4 and ClC-5. Nature *436*, 420–423.
47. Rost, B.R., Schneider, F., Grauel, M.K., Wozny, C., Bentz, C., Blessing, A., Rosenmund, T., Jentsch, T.J., Schmitz, D., Hegemann, P., and Rosenmund, C. (2015). Optogenetic acidification of synaptic vesicles and lysosomes. Nat. Neurosci. *18*, 1845–1852.
48. Kida, Y., Uchida, S., Miyazaki, H., Sasaki, S., and Marumo, F. (2001). Localization of mouse CLC-6 and CLC-7 mRNA and their functional complementation of yeast CLC gene mutant. Histochem. Cell Biol. *115*, 189–194.
49. Kasper, D., Planells-Cases, R., Fuhrmann, J.C., Scheel, O., Zeitz, O., Ruether, K., Schmitt, A., Poët, M., Steinfeld, R., Schweizer, M., et al. (2005). Loss of the chloride channel ClC-7 leads to lysosomal storage disease and neurodegeneration. EMBO J. *24*, 1079–1091.
50. Wartosch, L., Fuhrmann, J.C., Schweizer, M., Stauber, T., and Jentsch, T.J. (2009). Lysosomal degradation of endocytosed proteins depends on the chloride transport protein ClC-7. FASEB J. *23*, 4056–4068.
51. Yamamoto, T., Shimojima, K., Sangu, N., Komoike, Y., Ishii, A., Abe, S., Yamashita, S., Imai, K., Kubota, T., Fukasawa, T., et al. (2015). Single nucleotide variations in *CLCN6* identified in patients with benign partial epilepsies in infancy and/or febrile seizures. PLoS ONE *10*, e0118946.
52. Rohrbough, J., Nguyen, H.N., and Lamb, F.S. (2018). Modulation of ClC-3 gating and proton/anion exchange by internal and external protons and the anion selectivity filter. J. Physiol. *596*, 4091–4119.
53. Novarino, G., Weinert, S., Rickheit, G., and Jentsch, T.J. (2010). Endosomal chloride-proton exchange rather than chloride conductance is crucial for renal endocytosis. Science *328*, 1398–1401.
54. Weinert, S., Jabs, S., Supanchart, C., Schweizer, M., Gimber, N., Richter, M., Rademann, J., Stauber, T., Kornak, U., and Jentsch, T.J. (2010). Lysosomal pathology and osteopetrosis upon loss of H^+-driven lysosomal Cl^- accumulation. Science *328*, 1401–1403.
55. Weinert, S., Gimber, N., Deuschel, D., Stuhlmann, T., Puchkov, D., Farsi, Z., Ludwig, C.F., Novarino, G., López-Cayuqueo, K.I., Planells-Cases, R., and Jentsch, T.J. (2020). Uncoupling endosomal CLC chloride/proton exchange causes severe neurodegeneration. EMBO J. *39*, e103358.
56. Sekine, T., Komoda, F., Miura, K., Takita, J., Shimadzu, M., Matsuyama, T., Ashida, A., and Igarashi, T. (2014). Japanese Dent disease has a wider clinical spectrum than Dent disease in Europe/USA: genetic and clinical studies of 86 unrelated patients with low-molecular-weight proteinuria. Nephrol. Dial. Transplant. *29*, 376–384.
57. Bignon, Y., Alekov, A., Frachon, N., Lahuna, O., Jean-Baptiste Doh-Egueli, C., Deschênes, G., Vargas-Poussou, R., and Lourdel, S. (2018). A novel *CLCN5* pathogenic mutation supports Dent disease with normal endosomal acidification. Hum. Mutat. *39*, 1139–1149.
58. Kodama, H., Fujisawa, C., and Bhadhprasit, W. (2012). Inherited copper transport disorders: biochemical mechanisms, diagnosis, and treatment. Curr. Drug Metab. *13*, 237–250.
59. Hartwig, C., Zlatic, S.A., Wallin, M., Vrailas-Mortimer, A., Fahrni, C.J., and Faundez, V. (2019). Trafficking mechanisms of P-type ATPase copper transporters. Curr. Opin. Cell Biol. *59*, 24–33.
60. Kaler, S.G., Holmes, C.S., Goldstein, D.S., Tang, J., Godwin, S.C., Donsante, A., Liew, C.J., Sato, S., and Patronas, N. (2008). Neonatal diagnosis and treatment of Menkes disease. N. Engl. J. Med. *358*, 605–614.
61. Gaxiola, R.A., Yuan, D.S., Klausner, R.D., and Fink, G.R. (1998). The yeast CLC chloride channel functions in cation homeostasis. Proc. Natl. Acad. Sci. USA *95*, 4046–4050.
62. Hechenberger, M., Schwappach, B., Fischer, W.N., Frommer, W.B., Jentsch, T.J., and Steinmeyer, K. (1996). A family of putative chloride channels from *Arabidopsis* and functional complementation of a yeast strain with a *CLC* gene disruption. J. Biol. Chem. *271*, 33632–33638.
63. Schwappach, B., Stobrawa, S., Hechenberger, M., Steinmeyer, K., and Jentsch, T.J. (1998). Golgi localization and functionally important domains in the NH_2 and COOH terminus of the yeast CLC putative chloride channel Gef1p. J. Biol. Chem. *273*, 15110–15118.
64. Massie, H.R., Ofosu-Appiah, W., and Aiello, V.R. (1993). Elevated serum copper is associated with reduced immune response in aging mice. Gerontology *39*, 136–145.
65. Günther, W., Lüchow, A., Cluzeaud, F., Vandewalle, A., and Jentsch, T.J. (1998). ClC-5, the chloride channel mutated in Dent's disease, colocalizes with the proton pump in endocytotically active kidney cells. Proc. Natl. Acad. Sci. USA *95*, 8075–8080.
66. Günther, W., Piwon, N., and Jentsch, T.J. (2003). The ClC-5 chloride channel knock-out mouse - an animal model for Dent's disease. Pflugers Arch. *445*, 456–462.
67. Jentsch, T.J. (2007). Chloride and the endosomal-lysosomal pathway: emerging roles of CLC chloride transporters. J. Physiol. *578*, 633–640.
68. Chakraborty, K., Leung, K., and Krishnan, Y. (2017). High lumenal chloride in the lysosome is critical for lysosome function. eLife *6*, e28862.
69. Li, X., Wang, T., Zhao, Z., and Weinman, S.A. (2002). The ClC-3 chloride channel promotes acidification of lysosomes in CHO-K1 and Huh-7 cells. Am. J. Physiol. Cell Physiol. *282*, C1483–C1491.

70. Nicoli, E.R., Weston, M.R., Hackbarth, M., Becerril, A., Larson, A., Zein, W.M., Baker, P.R., 2nd, Burke, J.D., Dorward, H., Davids, M., et al.; Undiagnosed Diseases Network (2019). Lysosomal Storage and Albinism Due to Effects of a De Novo *CLCN7* Variant on Lysosomal Acidification. Am. J. Hum. Genet. *104*, 1127–1138.
71. Freeman, S.A., and Grinstein, S. (2018). Resolution of macropinosomes, phagosomes and autolysosomes: Osmotically driven shrinkage enables tubulation and vesiculation. Traffic *19*, 965–974.
72. Freeman, S.A., Uderhardt, S., Saric, A., Collins, R.F., Buckley, C.M., Mylvaganam, S., Boroumand, P., Plumb, J., Germain, R.N., Ren, D., and Grinstein, S. (2020). Lipid-gated monovalent ion fluxes regulate endocytic traffic and support immune surveillance. Science *367*, 301–305.